Journal of Applied Electrochemistry **32**: 661–670, 2002.

Monitoring hydrogen absorption in Pd electrodes by means of electric and electrochemical signals

A. VERTOVA, S. RONDININI and G. BUSCA*
Department of Physical Chemistry and Electrochemistry, University of Milan, via Golgi 19, I-20133 MILANO, Italy
**Present address: Krugg SpA, Via dei Lavoratori, 7, 20090 Buccinasco (MI), Italy*

Received 12 October 2001; accepted in revised form 19 March 2002

Key words: electric resistance, electrode potential, hydrogen, hydrogen monitoring, palladium

Abstract

A reliable, nondestructive methodology to determine the actual hydrogen content in hydrogen storage electrodes has been developed. This methodology is based on relative electric resistance measurements, backed up by measurements of electrode potential, since both quantities are or are derived from electric signals, easy to handle and use in automatic data acquisition lines. The setup and procedure for relative resistance measurements, both under electrolysis and at open circuit conditions, will be described and discussed in terms of possible error sources and their relevant uncertainties, on the basis of the results obtained for the Pd–H system, chosen as model system. The use of electric and electrochemical signals to determine the current–potential distribution along the electrode as a function of the cell geometry and the working conditions will also be presented.

List of symbols

d	distance from the working electrode (cm)
d'	initial distance of the Luggin tip from the working electrode (cm)
d_{app}	apparent distance of the Luggin tip from the working electrode (cm)
F	faradaic constant (C (mole of electrons)$^{-1}$)
I_{long}	d.c. current intensity applied longitudinally to the sample (mA)
$I_{long,tot}$	total d.c. current intensity applied longitudinally to the sample (mA)
I_{cell}	electrolysis current intensity (mA)
j	local current density (mA cm^{-2})
j_{cell}	electrolysis current density (mA cm^{-2})
K	$R_{Au}/R_{0,T_0}$ ratio
L	length of the sample wire (cm or mm)
n_{Pd}	mol Pd in the sample
p_{H_2}	partial pressure of hydrogen (Pa)
Q_t	quantity of charge (C)
r_0	radius of the sample wire (cm or mm)
R_{Au}	electric resistance of the Au terminals (mΩ)
R_x	true electric resistance at the loading ratio x (mΩ)
$R_{x,T}$	true electric resistance at the loading ratio x and at the working temperature T (mΩ)
R_{x,T_0}	true electric resistance at the loading ratio x and at the reference temperature T_0 (mΩ)
R_0	true electric resistance at $x = 0$ (mΩ)
R_{0,T_0}	true electric resistance at $x = 0$ and the reference temperature T_0 (mΩ)
R_{long}	noncorrected electric resistance at the loading ratio x (mΩ)
$R_{long,0}$	noncorrected electric resistance at $x = 0$ (mΩ)
R_x/R_0	true relative electric resistance
$R_{long}/R_{long,0}$	noncorrected relative electric resistance
S_t	wire cross section (cm^2)
t_0	starting time of discharge (s or min)
t_f	final time of discharge (s or min)
t_l	loading time (s or min)
U_d	potential at distance d from the working electrode (V)
$U_{d'}$	potential at distance d' from the working electrode (V)
U_0	potential at the working electrode surface (V)
U_{long}	potential difference at the loading ratio x (mV)
$U_{long,T}$	potential difference at the loading ratio x and at the working temperature T (mV)
$U_{long,0}$	potential difference at $x = 0$ (mV)
$U_{long,0,T_0}$	potential difference at $x = 0$ and at the reference temperature T_0 (mV)
U_{ref}	electrode potential (V)
x	H/Pd molar ratio or loading ratio

Greek symbols

α	temperature coefficient for the electric resistance of the Pd–Au system (°C^{-1})
α, β	phases of the system Pd–H
κ	specific conductance of the electrolyte (Ω^{-1} cm^{-1})
ρ_{Au}	resistivity of Au ($\mu\Omega$ cm)

1. Introduction

Hydrogen storage electrodes represent one of the most interesting and promising technological innovations in applied electrochemistry [1–16] their use ranging from battery [8–10] and fuel cell [6, 7, 11] electrodes, to anodes in electrolysers [12, 13] and gas sensors [14–16]. In accordance to the fields of application, different characteristics might be privileged. For instance, high electron transfer rates and absence of multiple phase regions are fundamental for both electrodic processes of loading and unloading and for reversibility of 'sensor' electrodes, while high absorption capacity and high diffusion rates of hydrogen into the electrodic mass are crucial only for current-driven processes.

Whatever the target application, it is of primary interest to develop reliable, nondestructive methodologies to determine the charging degree of the electrode whether it is under working conditions or stored for future use, and to select the best loading procedures for reaching the desired H/metal molar ratio while retaining mechanical and dimensional stability.

Among the physico-chemical parameters which characterize the electrode behaviour, we focused our attention on the relative electric resistance and on the electrode potential, since both are or are derived from electric signals, easy to handle and use in automatic data acquisition lines. Although both quantities have been already applied previously [17–25] and recently [26–29] to the study of the Pd–hydrogen (H and its isotopes) system, their simultaneous determination and its synergistic advantages were never described. Moreover, to our knowledge, the whole procedure for obtaining reliable and accurate resistance measurements on hydrogen storage electrodes, especially under working conditions, was never fully elucidated.

The aim of this work is to present and discuss the apparatus and the relevant signal handling procedure for obtaining reliable, low-cost, online information on the status of the hydrogen–metal system by means of relative resistance measurements both under electrolysis and at open circuit conditions, and to show how this parameter can be fruitfully correlated to the electrode potential, a signal which unfortunately might suffer the limitations implicit in the presence of a biphasic zone, as in the model case of Pd–H.

The present discussion will cover the combined use of electric and electrochemical signals for the following selected applications: online monitoring of H/Pd molar ratio, x; determination of the current–potential distribution along the electrode as a function of the cell geometry and the working conditions; selection of the best working conditions for electrode charging and discharging; and redetermination of the 'α-Pd' reversible electrode potential frequently used instead of the classic Pt–H_2 electrode when in the presence of easily hydrogenable substrates [30].

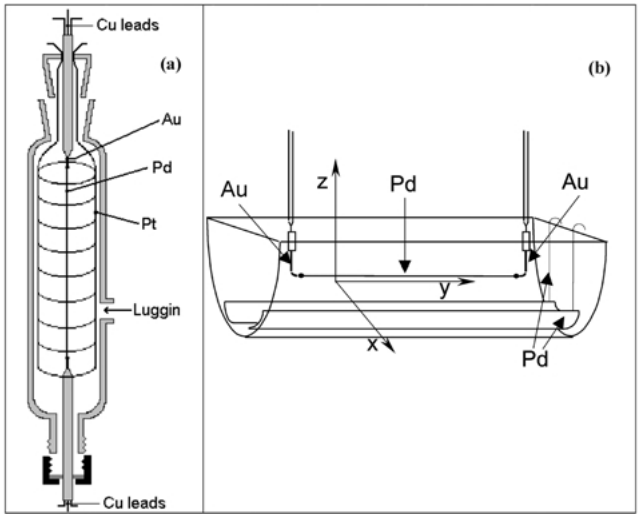

Fig. 1. Cell schemes. (a) Cell 1 used to optimize the relative electric resistance measurements; (b) cell 2 used together with a mobile Luggin probe (not shown) for potential measurements under controlled charging/discharging conditions.

2. Experimental details

The two different all-glass cells (cell 1 and cell 2) used are illustrated in Figures 1(a) and (b). Cell 1 was used for determining the relative resistance–x relationship, at $T = 25$ °C, while cell 2 was used for current–potential distribution determinations, at room temperature. This latter cell, in fact, allowed accurate (<0.1 mm) and reproducible positioning of the Lugging tip of the reference electrode along and around the specimen, by means of micrometric screws (not shown). Figure 2 shows the instrumentation setup, used to drive the experiments and to simultaneously acquire the relevant cell parameters; the scheme applies to both cells.

Resistance measurements (cell 1) were carried out in H_2SO_4 0.1 mol kg^{-1} aqueous solutions while loading cathodically a Pd wire (Engelhard, flame annealed, dia. 0.5 mm, 4 cm $\leqslant L \leqslant$ 8 cm), the counter electrode

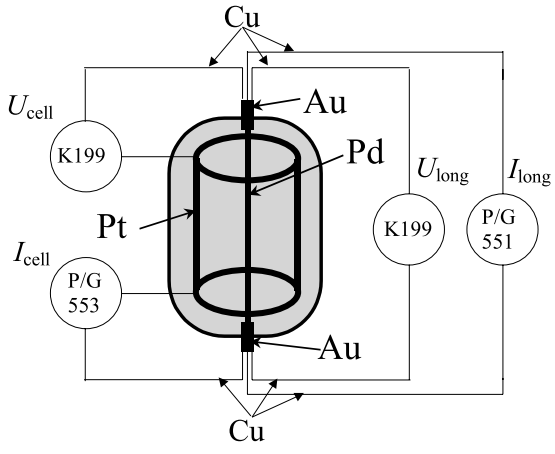

Fig. 2. Scheme of cell and apparatus set-up used to perform the experiments and to monitor the process variables indicated in correspondence of the relevant instrumentation (in circles).

being a Pt cage. The sample was suspended in the axial position by means of two short (1 cm), spot welded Au rods (dia. 1 mm), which in turn were welded into two glass tubes used for shielding and mounting purposes. The gold terminals were used to prevent any hydrogen loss from Pd other than toward the solution. Four terminal resistance measurements were performed by feeding along the wire a direct current (d.c.) (I_{long} = 32 mA) by means of an AMEL 551 potentiostat/galvanostat (P/G 551 in Figure 2) and by monitoring the resulting potential difference (p.d.) along the palladium wire (U_{long}) by means of a Keithley multi-meter model 199 (K199). In the earlier stages of the experiments an alternating square-wave I_{long} signal (Datatranslation® interface, DT2801, period 480 ms) was used while simultaneously recording U_{long} at selected intervals (400 readings in the last 40 ms of each half-period) to avoid asymmetry contributions due to, thermoelectric effects etc. Having carefully checked that the d.c. measurements gave the same results with comparable accuracy, provided that the d.c. current intensity is kept sufficiently low, the square-wave method was discontinued. The electrolyses were performed either at constant current (I_{cell}) or at constant electrode potential (U_{ref}), using a 'quinhydrone' reference electrode [31], by means of an Amel 553 potentiostat/galvanosat (P/G 553); the above signals and the cell voltage (U_{cell}) were monitored by means of K199. The temperature, T, of the solution was also monitored using a K-type thermocouple (not shown in the Figures) with the reference junction at 0 °C. All signals were recorded with the K199 connected to a personal computer (*via* an IEEE488 card) for automatic data acquisition.

In cell 1 the sample wire was kept straight by means of a spring fastened to the ceiling of the thermostatting chamber. The quinhydrone reference electrode was connected to the cell by means of a Luggin tip *via* a syringe-type insertion point, as indicated by the arrow in Figure 1(a).

Current–potential distribution determinations (cell 2) were carried out in H_2SO_4 0.1 mol kg^{-1} aqueous solutions, using as cathode a Pd wire (dia. 0.5 mm, length $L \approx 5$ cm), connected to the external leads through two spot welded gold terminals 1–2 cm long, and as anode two long Pd foils positioned on the bottom of the cell (Figure 1(b)). A mobile Luggin tip (not shown), which allowed to monitor the cathode potential along and around the palladium wire, was fixed to a platform which controlled the position of the Luggin in the following three different directions: along the wire, y axis; horizontal movement, x axis; and vertical movement, z axis. For example, the position $x, y, z = 0, 0, 0$ corresponds to the starting position, that is the end of the Pd wire to which the d.c. power supply connexions for I_{cell} and I_{long} (negative terminal) were made; $x, y, z = 0, L, 0$ identifies the other extremity of the L cm long wire. Due to hydrogen absorption, the sample increases in length by about 3.5% during the loading period, flexes and resumes its straight position only after complete unloading. Because of this cyclic deformation, the x and z coordinates are relative to the actual position of the wire during the charging/discharging cycle.

3. Results and discussion

The relative electric resistance is defined as the ratio between the resistance, R_x, of the sample at the loading degree x, and the resistance of the sample at $x = 0$, R_0. In principle, the simple following equation could be applied:

$$\frac{R_{long}}{R_{long,0}} = \frac{U_{long}}{I_{long}} \times \frac{I_{long}}{U_{long,0}} = \frac{U_{long}}{U_{long,0}} \quad (1)$$

where $U_{long,0}$ and U_{long} represent the p.d. along the sample at $x = 0$ and during loading, respectively, $R_{long,0}$ and R_{long} are correspondingly the electric resistances, and I_{long} is the intensity of the d.c. current applied longitudinally to the sample. The selected I_{long} value (32 mA) proved to be high enough to give reliable voltage drops (at $I_{cell} = 0$, U_{long} readings are of a few millivolts with a typical uncertainty of 3–4 μV), but not too high to produce any significant temperature effect. Equation 1 also points out how easy could be an online monitoring of the relative resistance, by monitoring the two I_{long} and U_{long} signals.

However, the quantity calculated by means of Equation 1 differs from the sought R_x/R_0 value because it is affected by three contributions that must be taken into account to perform reliable, online relative resistance measurements; namely, (i) loading/unloading current intensity; (ii) temperature effect; and (iii) gold terminals.

The corrections to be performed are therefore discussed here below.

3.1. *Electrolytic current*

While the quantity $U_{long,0}$ is measured in presence of the longitudinal current only, the quantity U_{long} is recorded also in presence of the electrolysis current, I_{cell}.

Although any co-conduction effect can be excluded, that is, any partial I_{long} leakage through the electrolyte [20, 32] because measurements are carried on thick samples (dia. 0.5 mm) and using direct current, the additional potential difference generated by the charging/discharging current must be duly accounted for, as already pointed out in the case of thin film electrodes [33]. In our case, it can be easily demonstrated that the contribution of I_{cell} to the total longitudinal current $I_{long,tot}$ is a linear function of I_{cell}, given by the following equation:

$$I_{long,tot} = I_{long} + f(I_{cell}) = I_{long} + 0.5 \times I_{cell} \quad (2)$$

which is valid for both homogeneous and nonhomogeneous I_{cell} distribution provided that in case of

inhomogeneity the current presents a plane of symmetry in $L/2$ (see Appendix).

Accounting for this correction the wire resistance at the working temperature, $R_{x,T}$, is given by

$$R_{x,T} = \frac{U_{\mathrm{long},T}}{I_{\mathrm{long,tot}}} = \frac{U_{\mathrm{long},T}}{I_{\mathrm{long}} + 0.5 \times I_{\mathrm{cell}}} \tag{3}$$

where $U_{\mathrm{long},T}$ denotes the longitudinal p.d. at the working temperature T.

It is possible to experimentally evaluate the contribution of I_{cell} to the longitudinal current by varying I_{long} while keeping I_{cell} constant; in fact at $U_{\mathrm{long},T} = 0$, $I_{\mathrm{long,tot}}$ is accordingly null, hence from Equation 2 one should obtain $-I_{\mathrm{long}} = 0.5 \times I_{\mathrm{cell}}$. Experimentally, the average of the slopes obtained in this way is 0.490 ± 0.025, thus confirming that the electrolysis current distribution along the sample is satisfactorily homogeneous.

According to Equation 3, neglecting the longitudinal component of I_{cell} results in R_{long} values higher than the corresponding $R_{x,T}$ by a factor equivalent to $(I_{\mathrm{long}} + 0.5 \times I_{\mathrm{cell}})/I_{\mathrm{long}}$. In our experiments the $R_{\mathrm{long}}/R_{x,T}$ ratio ranged from 1.1 to 3.3 in dependence on the I_{cell} values (typically 10–150 mA).

3.2. *Temperature*

Although all the experiments were performed in an air thermostat to ensure a constant temperature, the actual temperature of the cell might differ from that of the chamber because of the heat dissipated during the electrolytic charging/discharging process, in dependence on the applied current intensity. Obviously, the higher the current the higher the temperature effect on the sample. Therefore, while the measure of R_0 was carried out at $I_{\mathrm{cell}} = 0$, and hence at the reference temperature T_0 ($T_0 = 25$ °C), $R_{x,T}$ was carried out during the electrolytic process at the temperature T, whose difference from T_0 must be duly accounted for. As for a resistance thermometer, the dependence of the electric resistance on temperature, for $\Delta T \leqslant 50$ °C, can be expressed as follows:

$$R_{x,T_0} = R_{x,T}[1 - \alpha(T - T_0)] \tag{4}$$

where α is the temperature coefficient of the metal system, which was experimentally determined for the Pd–Au system and found to be $\alpha = 0.003\ (^{\circ}\mathrm{C})^{-1}$ [34].

Hence, the relative electric resistance is given by

$$\frac{R_{x,T_0}}{R_{0,T_0}} = \left\{ \frac{U_{\mathrm{long},T}}{I_{\mathrm{long}} + 0.5 \times I_{\mathrm{cell}}} [1 - \alpha(T - T_0)] \right\} \frac{I_{\mathrm{long}}}{U_{\mathrm{long},0,T_0}} \tag{5}$$

The temperature has little effect; in fact, no recorded ΔT value was greater than 0.5 °C, its contribution never exceeded a $R_{x,T}/R_{x,T_0}$ ratio equal to 1.0015.

3.3. *Au terminals*

As described in Section 2, short Au rods (dia. 1 mm, total length $\simeq 2$ cm) were inserted between the Pd wire and the outer Cu leads to avoid loss of hydrogen by diffusion and to reduce the mechanical stress on glass tubes sustaining the entire cathode structure (Figure 1(a)). Gold wires introduce an additive resistance, which is independent of the loading level and which must be accounted for.

Then the true relative resistance can be expressed as

$$\frac{R_x}{R_0} = \frac{R_{x,T_0} - R_{\mathrm{Au}}}{R_{0,T_0} - R_{\mathrm{Au}}} \tag{6}$$

where R_{Au}, the resistance of the gold wires, can be calculated from the geometric characteristics and from the resistivity of gold at $T = T_0 = 25.0$ °C: $\rho_{\mathrm{Au}} = 2.49\ \mu\Omega$ cm [35].

Equation 6 then becomes

$$\frac{R_x}{R_0} = \frac{1}{1 - K} \times \frac{R_{x,T_0}}{R_{0,T_0}} - \frac{K}{1 - K} \tag{7}$$

where K denotes the $R_{\mathrm{Au}}/R_{0,T_0}$ ratio, which, for our samples, is about 0.1.

Thus, neglecting the Au contribution produces an underestimation of the true R_x/R_0 value; in fact, the $(R_{x,T_0}/R_{0,T_0})/(R_x/R_0)$ ratio decreases from 1 to 0.95 for R_x/R_0 ranging from 1 to 1.8.

3.4. *True relative resistance and loading ratio*

Summarizing all the contributes, the true relative resistance is given by

$$\frac{R_x}{R_0} = \frac{1}{1 - K} \left\{ \frac{U_{\mathrm{long},T}}{I_{\mathrm{long}} + 0.5 \times I_{\mathrm{cell}}} [1 - \alpha(T - T_0)] \right\} \times \frac{I_{\mathrm{long}}}{U_{\mathrm{long},0,T_0}} - \frac{K}{1 - K} \tag{8}$$

which can be used to perform real-time reelaboration of the raw U and I signals within the data acquisition cycle.

Figures 3 and 4 show how deeply the true relative resistances (right ordinate, continuous lines) can differ from the raw $R_{\mathrm{long}}/R_{\mathrm{long},0}$ values (left ordinate, dotted lines) during loading (Figure 3(a) and 3(b)) and unloading (Figure 4) cycles. They emphasize how the described corrections are important in obtaining reliable R_x/R_0 values to be used for monitoring the hydrogen content of the palladium wire.

Unloading is performed at constant potential, hence the discharging rate is almost similar for all the samples, but loading is galvanostatic and different I_{cell} values produce different loading rates, as underlined in Figure 3(a) and (b) where the data relevant to two different charging currents are presented; namely, $I_{\mathrm{cell}} = 30$ mA and $I_{\mathrm{cell}} = 90$ mA. Although the charging and discharging processes could be qualitatively followed by moni-

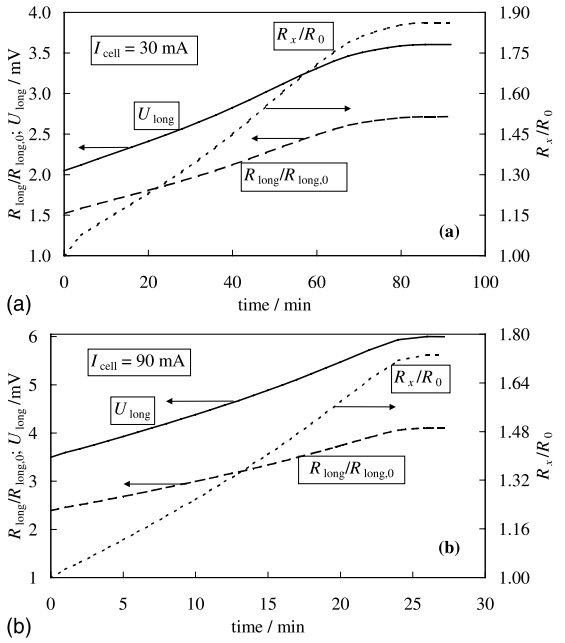

Fig. 3. True relative electric resistance, R_x/R_0, (dotted line, right axis), raw relative electric resistance, $R_{long}/R_{long,0}$, (dashed line, left axis) and p.d. between the ends of Pd wire, U_{long}, (continuous line, left axis) during the charging half-cycle at two different current intensities. (a) $I_{cell} = 30$ mA and (b) $I_{cell} = 90$ mA.

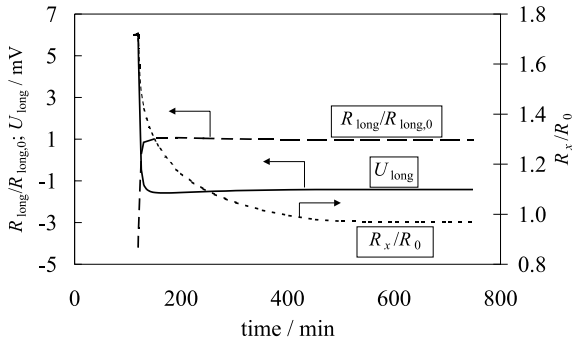

Fig. 4. True relative electric resistance, R_x/R_0, (dotted line, right axis), raw relative electric resistance, $R_{long}/R_{long,0}$, (dashed line, left axis) and p.d. between the ends of Pd wire, U_{long}, (continuous line, left axis) during the controlled potential discharge half-cycle.

toring the raw signal U_{long} (also quoted in Figures 3 and 4, left ordinate), the quantitative determination of the H/Pd ratio needs the true relative resistance values to apply the R_x/R_0 against x relationship derived as described below. Figure 3 also shows that the loading step is roughly divided into two periods: at first R_x/R_0 increases almost linearly with time (linear region), with a slope depending on the charging current density; then, above a certain loading level (see below) R_x/R_0 becomes almost constant (plateau region) due to slackness of further hydrogen absorption.

During the unloading process presented in Figure 4, R_x/R_0 decreases with time together with the decrease of I_{cell} since the discharge was driven potentiostatically to evaluate the loading ratio x as

$$x = \left[\frac{H}{Pd}\right]_t = \frac{Q_t/F}{n_{Pd}} \tag{9}$$

Q_t being the residual charge quantity calculated as

$$Q_t = \int_{t_0}^{t_f} I_{cell}\mathrm{d}t - \int_{t_0}^{t} I_{cell}\mathrm{d}t$$

where t_0 and t_f denote, respectively, the starting and the final time of unloading; F is the faradaic constant (96 485.309 C (mol of electrons)$^{-1}$) and n_{Pd} the number of moles of Pd sample.

The potentiostatic unloading used for the evaluation of x through Equation 9 was performed at $U_{ref} \simeq -400/-200$ mV vs quinhydrone, to ensure that the only electrode reaction is the oxidation of H in H^+ and guarantee unit current efficiency.

In Figure 5 the characteristics R_x/R_0 against x is presented. The interpolating curve is obtained by using the Mathematica® software and a multilinear regression method to give following equation:

$$\frac{R_x}{R_0} = ax^4 + bx^3 + cx + d \tag{10}$$

with $a = -2.17 \pm 0.12$; $b = 2.21 \pm 0.14$; $c = 0.649 \pm 0.044$; $d = 1.0041 \pm 0.0037$; root mean square error (RMSE) = 0.014; $R^2 = 0.998$.

The R_x/R_0 values are in good agreement with those determined by Smith and Otterson [25], even if we never observed any decrease in R_x/R_0 at the highest x values, not even under prolonged electrolysis conditions. Surface modifications connected with the presence of Na_2S and formaldehyde in the Smith and Otterson electrolyte might possibly account for this discrepancy. In fact, chemisorption of sulfide species is known to affect surface coverage by adsorbed H on transition metals and, as recently pointed out by Qian, Conway and Jerkiewicz [29], can affect the subsurface concentration of hydrogen and hence the total hydrogen content. As is well established, at increasing concentration of interstitially dissolved (octahedral sites) H the Pd 4d-band is

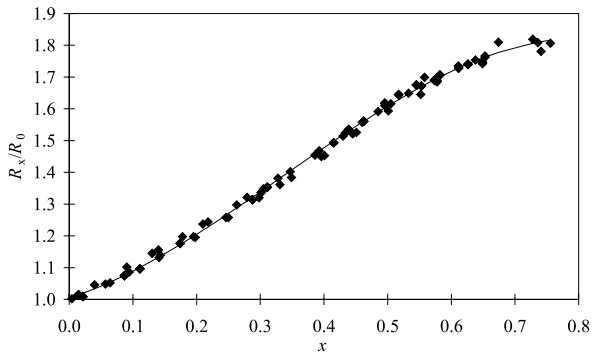

Fig. 5. True relative electric resistance, R_x/R_0, as a function of the H/Pd loading ratio, x.

increasingly occupied, thus producing the observed increase of the R_x/R_0 ratio and modifying at the same time the magnetic properties of the material, which becomes almost diamagnetic for H/Pd $\geqslant$ 0.7 [36]. In turn, this would enhance the conductivity of the system which, for further increase of the hydrogen content above this threshold, and very likely above the 1–1.2 loading ratio [37], would produce a sudden decrease in the R_x/R_0 values, as observed by Smith and Otterson.

Earlier R_x/R_0 against x data reported by Sieverts and Danz [18] are significantly different, especially for $x \geqslant 0.3$; but no explanation can be offered in this case, because of total lackness of experimental details.

Now, applying Equation 10 to the charging step of the loading/unloading cycle, one can summarize the results obtained for each selected value of I_{cell} by plotting R_x/R_0 and U_{ref} against time as shown in Figure 6, where the time domains of the α, $\alpha + \beta$ and β phases have also been added (the vertical lines mark the times at which the $x = \alpha_{max} = 0.008$ and $x = \beta_{min} = 0.607$ values are reached, at room temperature [38]). It can be noticed that until the β phase is reached R_x/R_0, and hence the loading level x, change almost linearly with time, thus emphasizing that in this region the process of hydrogen absorption has a 100% current efficiency.

It can also be seen that the electrode potential, U_{ref}, has a trend similar to the adsorbing isotherms of the Pd/H system [36], although the characteristic plateau relative to the α–β transition is shifted by some 30 mV due to the contribution of the IR drop between the Luggin tip and the surface of the sample.

Since the hydrogen charging ratio, x, can be reliably determined by four-terminal resistance measurements, upon performing the described reelaboration procedure of the recorded signals, the correlation between the electrode potential and x (or, equivalently, R_x/R_0) during the loading period can be studied by means of the apparatus presented in Figure 1(b), by which it was possible to carefully control the distance of the Luggin tip from the wire.

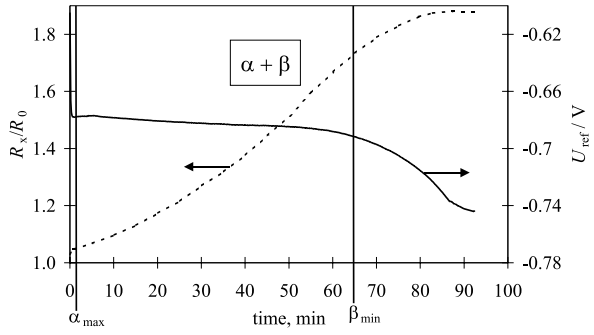

Fig. 6. True relative electric resistance, R_x/R_0, (dotted line, left axis) and electrode potential, U_{ref} vs quinhydrone, (continuous line, right axis) as a function of time during a charging half-cycle at $I_{cell} = 30$ mA. The vertical lines mark the time domains of the α, $\alpha + \beta$ and β phases, respectively.

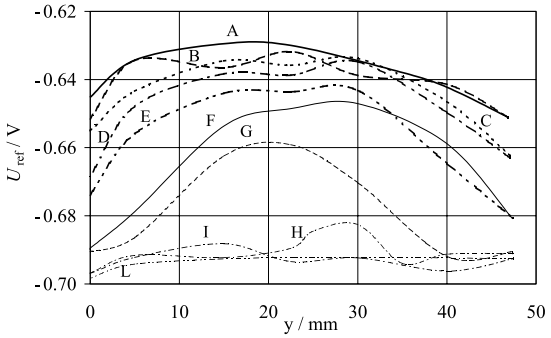

Fig. 7. Electrode potential, U_{ref} vs quinhydrone, along the wire as a function of the y position of the Luggin tip, at $x = z = 0$, for different charging times: (A) 13, (B) 21, (C) 28, (D) 51, (E) 59, (F) 72, (G) 79, (H) 89, (I) 100 and (L) 113 min.

3.5. *Electrode potential and loading ratio*

Different series of experiments were performed on different samples. In the first series, the U_{ref} signal was recorded by moving the Lugging tip along the Pd cathode (y axis) at $x = z = 0$, under charging conditions at different current densities. As shown by the curves in Figure 7, recorded at $j_{cell} = 15.3$ mA cm^{-2} at different electrolysis times, the loading apparently starts from the extremities of the wire, as more negative U_{ref} values should denote higher local H/Pd ratios. This inhomogeneity apparently dissolves after some time, as shown by curve L, when the centre of the wire reaches the same potential of the extremities, and concomitantly R_x/R_0 reaches its maximum value, thus indicating that the whole wire is now completely charged. This condition still exists at the highest current densities investigated ($j_{cell} = 76.1$ mA cm^{-2}), even if the required time is shorter.

This behaviour points to a nonhomogeneous current distribution along the wire, whose symmetry with respect to $L/2$ closely resembles a secondary current distribution profile [39], which levels off at increasing electrode potentials. Note that for a symmetric although inhomogeneous current distribution Equation 2, and hence Equation 8, still holds, as demonstrated in the Appendix. To confirm this hypothesis a second series of experiments was performed by recording the electrode potentials, under charging conditions $j_{cell} = 60.3$ mA cm^{-2} in the R_x/R_0 plateau region, where U_{ref} variations cannot be attributed to changes in H/Pd composition, at three different y values (namely, at the two extremities and in the centre of the wire), while varying the distance of the Luggin tip along the other two axes (i.e., horizontally x, vertically z). This allowed to obtain the potential distribution around the wire for the three different constant y planes, as shown in Figure 8 for the $y = 20$ mm. The terms 'z up' and 'z down', used here and in the following Table 1, denote the vertical positions of the Luggin tip *above* and *below* the wire, respectively.

The symbols in the Figure represent the recorded U_{ref} values, while the continuous lines are the corresponding

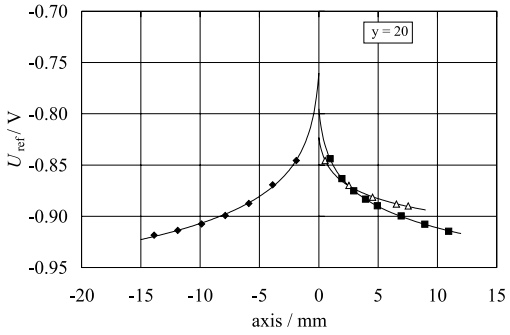

Fig. 8. Potential distribution around the sample wire under charging conditions in the R_x/R_0 *plateau* region, as a function of the horizontal, x, and vertical, z, distance from the electrode, at $y = 20$ mm. Key: (♦) z down; (△) z up; (■) x var.

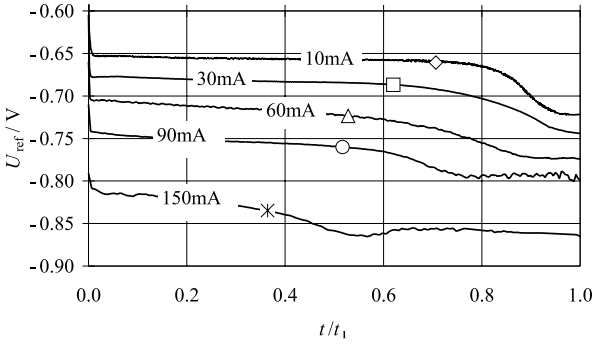

Fig. 9. Electrode potential, U_{ref} against the normalized loading time, t/t_l, at different electrolytic current intensities. Symbols mark the time instant at which starts the HER, in concurrence to the hydrogen absorption process. Corresponding loading ratios, x, are: (◇) 0.62, (□) 0.52, (△) 0.43, (◯) 0.38 and (☆) 0.33. Potentials are measured *vs* quinhydrone reference electrode.

values calculated by means of the following equation, which represents the variation of potential between a central wire working electrode and a coaxial cylindrical counter electrode as a function of the interelectrodic distance d [40]:

$$U_d = U_0 + \frac{j}{\kappa} r_0 \ln\left(\frac{r_0 + d}{r_0}\right) \tag{11}$$

where U_0 is the potential at the electrode surface (V); j is the local electrolytic current density (A cm^{-2}); κ is the specific conductance of the solution (0.030 26 Ω^{-1}cm^{-1}); and r_0 is the wire working radius (0.025 cm).

Since in the experimental set-up the Luggin tip cannot be in direct contact with the wire but is at an arbitrary starting 'zero' position, the distance d' between the electrode surface and the tip must be accounted for. So Equation 11 becomes

$$\begin{aligned} U_d &= U_{d'} + \frac{j}{\kappa} r_0 \ln\left(\frac{r_{app} + d_{app}}{r_{app}}\right) \\ &= U_0 + \frac{j}{\kappa} r_0 \ln\left(\frac{r_0 + d' + d_{app}}{r_0}\right) \end{aligned} \tag{12}$$

where $U_{d'} = U_0 + \frac{j}{\kappa} r_0 \ln(\frac{r_0 + d'}{r_0})$; $r_{app} = r_0 + d'$ is the apparent wire radius and $d_{app} = d - d'$ is the apparent distance from the wire.

Equation 12 allows the simultaneous determination of U_0, j and d' by a nonlinear regression method. The corresponding values, optimized with Mathematica® for each separate run, are collected in Table 1. The comparison between the reported local j values at the three different constant y planes shows that for any tip position, namely 'z down', 'z up' and 'x var', the highest current densities occur at the extremities ($y = 0$ and 50 mm), the 'z up' values, however, are always the smallest ones, as expected due to the particular cell 2 geometry. These results confirm the starting hypothesis of inhomogeneous current distribution along the wire, inhomogeneity which however never exceeds a factor of 2. Interestingly, the j values at the extremities are very close to the average applied current density ($j_{cell} = 60.3$ mA cm^{-2}), which is compatible with the supposed secondary current distribution profile, since the sample is connected using nonisolated gold contacts.

To underline the influence of current density on the charging level of palladium, electrolysis at different currents were performed, while monitoring U_{ref} with the Luggin probe positioned at 0, $L/2$, 0. The chosen intensities were $I_{cell} = 10$, 30, 60, 90 and 150 mA, which corresponded to $j_{cell} = 7.07$, 21.22, 42.44, 63.66 and 106.10 mA cm^{-2}. The recorded curves are reported in Figure 9 against the normalised loading time, t/t_l. On each of the five curves the symbols mark the first formation of bubbles along the wire. The correlation between these markers and x, whose values are shown in the legend, underlines that the higher the electrolysis current the lower the H/Pd ratio at which hydrogen evolution reaction starts up. In fact, at high charging current the absorption of hydrogen, and in particular its

Table 1. Potentials at the electrode surface, U_0 *vs* quinhydrone (V), local current densities, j (A cm^{-2}), and true initial distances of the Luggin tip from the electrode surface, d' (cm), as obtained by the nonlinear optimization of Equation 12, for the sample wire under charging conditions in the R_x/R_0 *plateau* region, for the nine series of experiments performed at different horizontal, x, and vertical, z, position of the Luggin tip, and at three different y planes: (a) $y = 0$ mm, (b) $y = 20$ mm and (c) $y = 50$ mm

	$y = 0$ mm			$y = 20$ mm			$y = 50$ mm		
	z down	z up	x var	z down	z up	x var	z down	z up	x var
U_0/V	−0.7480	−0.7421	−0.7383	−0.7602	−0.8231	−0.7950	−0.7485	−0.7680	−0.7134
j/Acm^{-2}	0.0581	0.0385	0.0600	0.0479	0.0237	0.0379	0.0606	0.0200	0.0693
d'/cm	0.0568	0.1536	0.0693	0.1890	0.0537	0.0943	0.0504	0.1968	0.1174

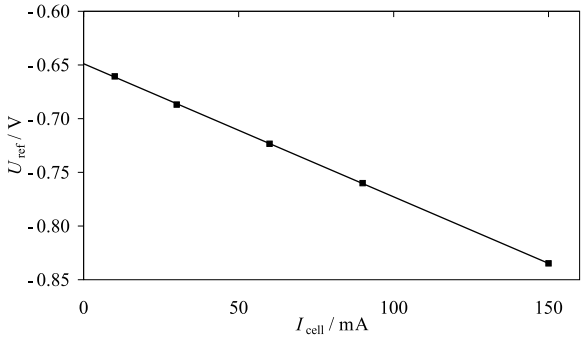

Fig. 10. Electrode potentials, U_{ref} vs quinhydrone, measured at the markers in Figure 9, as a function of the corresponding electrolytic current intensities. Calculated straight line equation: $U_{ref} = -0.6489 - 1.239\ I_{cell}$.

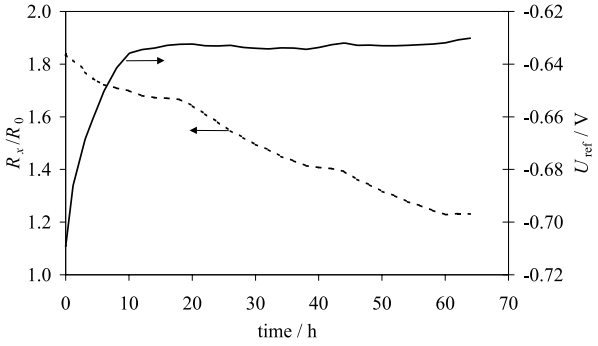

Fig. 12. True relative electric resistance, R_x/R_0, (dotted line, left axis) and electrode potential, U_{ref} vs quinhydrone, (continuous line, left axis) as a function of time during natural discharging, $I_{cell} = 0$, of a previously charged sample.

diffusion inside the metal, is slower than the production of atomic hydrogen; hence the outer metallic layers become readily saturated and the evolution of hydrogen takes place. This change from absorption to adsorption + evolution is then marked also by a change in the U_{ref} against time slope (see again the markers in Figure 9). These characteristic potential values linearly depend on the current intensity (Figure 10) and by extrapolating at $I_{cell} = 0$ it is possible to obtain the electrode potential under reversible conditions: $U_{ref} = -648.9$ mV vs quinhydrone, hence $U_{ref} = 51.1$ mV vs RHE, in good agreement with literature data [30] for an electrode with H/Pd ratio inside the $\alpha-\beta$ biphasic area. The slope of the straight line, 1.239 Ω, can then be used to substract the ohmic contribution of the solution from the electrode potential values recorded under electrolysis conditions, to give the curves in Figure 11, of corrected U_{ref} values against R_x/R_0. As can be clearly seen, the curves closely resemble the absorption isotherms, ln p_{H_2} against x. In fact, the relative resistance is almost linear with the hydrogen loading ratio, at least up to H/Pd ≈ 0.6, therefore, U_{ref} (which is proportional to ln p_{H_2}) is constant within the phase transition zone, especially at lower current densities when the slower and more homogeneous loading widens the *plateau* zone. As pointed out, at higher current density, the hydrogen evolution reaction (HER) begins at low values of relative resistance, which then represents the only significant parameter to monitor the loading extent. The inadequacy of U_{ref} in providing the actual H/Pd ratio is evident also for the unloading process, as shown in Figure 12, which refers to a natural ($I_{cell} = 0$) discharge step. In fact, after an initial rapid decreasing due to the depolarization and the immediate discharge of the outermost metal layers, the potential signal reaches a *plateau* as soon as the metal enters the transition phase, while the resistance signal still varies almost linearly during the entire unloading period (~60 h), until very low values are reached thus indicating correspondingly low hydrogen content ($R_x/R_0 \approx 1.2$, $x \approx 0.2$).

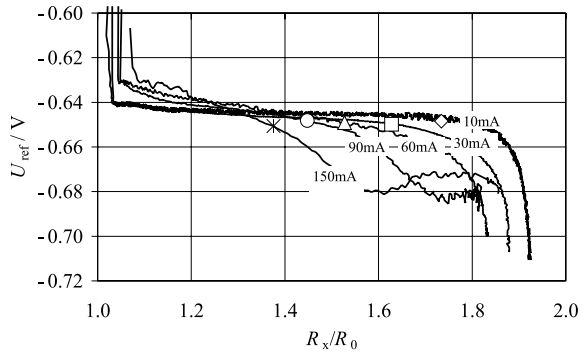

Fig. 11. Electrode potential, U_{ref} vs quinhydrone, *versus* the true relative electric resistance, R_x/R_0, after correction for the *IR* ohmic drop. Corresponding loading ratios, x, are: (◇) 0.62, (□) 0.52, (△) 0.43, (◯) 0.38 and (★) 0.33.

4. Conclusions

In summary, the relative resistance R_x/R_0 is a useful tool for the determination of the loading level of a hydride electrode, provided that the necessary corrections to the raw signals are applied. In fact, only upon performing the described reelaboration procedure, the four-terminal d.c. method becomes suitable for online monitoring and allows accurate *in situ* measurements during chemical or electrochemical loading/unloading cycles. The main error sources, which affect the raw signals, and come from the loading/unloading current intensity, the temperature and the metal terminals, have been expressed in term of the experimental variables and duly quantified.

The R_x/R_0 quantity can then be successfully used to drive the electrode at selected working conditions, even when the electrode potential is ineffective in providing the required information.

The R_x/R_0 against x characteristic for the Pd–H system at $T = 25$ °C in the $0 \leqslant x \leqslant 0.77$ range has also been redetermined and used to derive the U_{ref} against x (or against R_x/R_0) plots, which show the characteristic *plateau* of the $\alpha-\beta$ transition zone, equivalent to the p_{H_2} = constant in the Pd–H absorption isotherms. The rest value, generally referred to as the 'α–Pd' electrode potential, has been redetermined.

The procedure described is not only reliable and accurate, but also economically attractive and easily implementable and adaptable to different electrode geometries, and is therefore of general use and application for the study of other metal–hydride systems.

Acknowledgements

The financial support of the University of Milan is gratefully acknowledged.

Appendix

The electrolytic current is found to contribute to the total longitudinal current by $0.5 \times I_{cell}$, as expressed by Equation 2: $I_{long,tot} = I_{long} + f(I_{cell}) = I_{long} + 0.5 \times I_{cell}$.

In fact, considering a generic cross-section S of the sample wire, the longitudinal component $j_{t,y}$ cross-section S at y level of the electrolytic current density (j_{cell}) applied to the 'zero' end of the wire, is given by

$$j_{t,y} = \int_{y}^{L} \frac{j_{cell} C}{S} dy = \frac{I_{cell}}{S} \frac{L-y}{L} \tag{13}$$

where L is the length and C the circumference of the wire of radius r_0, and $j_{cell} = I_{cell}/(L \times C)$ is assumed homogeneous along the entire wire length.

Correspondingly, at the connecting point 'zero':

$$j_{t,0} = \int_{0}^{L} \frac{j_{cell} C}{S} dy = \frac{I_{cell}}{S} \tag{14}$$

The mean current density through the wire cross-section can then be calculated as

$$\langle j_t \rangle = \frac{1}{L} \int_{0}^{L} j_{t,y} dy = \frac{1}{L} \int_{0}^{L} \left(\int_{y}^{L} \frac{j_{cell} C}{S} dy \right) dy = \frac{1}{2} \frac{I_{cell}}{S} \tag{15}$$

hence the overall longitudinal current intensity which flows along the sample under electrolysis conditions, $I_{long,tot}$, for an homogeneous I_{cell} current distribution, can be readily calculated according to Equation 2.

It is worthwhile noting that Equation 15 would be valid even in presence of I_{cell} inhomogeneity provided that it presents a plane of symmetry at $L/2$. In fact, although the solution in Equation 13 is no longer valid since j_{cell} is not constant, the definition of the mean current density $\langle j_t \rangle$ implies:

$$\langle j_t \rangle = \frac{1}{L} \int_{0}^{L} j_{t,y} dy = \frac{1}{L} \lim_{N \to \infty} \sum_{1}^{N} \delta_i j_{t,i} \tag{16}$$

where $\delta_i = L/N$ represents the amplitude of the arbitrary interval into which the integration range can be subdivided, and $j_{t,i}$ is the value of the integral in Equation 13 evaluated at the ith level.

If j_{cell} is symmetric with respect to $L/2$ (that is $j_{cell}(y) = j_{cell}(-y)$), the following equivalences hold:

$$j_{t,y} + j_{t,L-y} = j_{t,0} = I_{cell}/S \tag{17}$$

since the summation in Equation 16 is extended over $N/2$ pairs $j_{t,y} + j_{t,L-y}$, it results:

$$\langle j_t \rangle = \frac{1}{L} \lim_{N \to \infty} \sum_{1}^{N} \delta_i j_{t,i} = \frac{1}{L} \frac{L}{N} \sum_{1}^{N} j_{t,i} = \frac{1}{L} \frac{L}{N} \frac{N}{2} \frac{I_{cell}}{S} = \frac{1}{2} \frac{I_{cell}}{S} \tag{18}$$

References

1. O.A. Petrii, I.V. Rovrigina and S.YA. Vasina, *Mater. Chem. Phys.* **22** (1989) 51.
2. K. Petrov, A.A. Rostami, A. Visintin and S. Srinivasan, *J. Electrochem. Soc.* **141** (1994) 1747.
3. P.H.L. Notten and P. Hokkeling, *J. Electrochem. Soc.* **138** (1991) 1877.
4. M. Matsuoka, T. Kohno and C. Iwakura, *Electrochim. Acta* **38** (1993) 787.
5. G.D. Adzic, J.R. Johnson, J.J. Reilly and H.S. Lim, *J. Electrochem. Soc.* **142** (1995) 3424.
6. M.E. Malinowski, and K.D. Stewart, Sandia National Laboratory Technical Report SAND97-8289, Sandia National Laboratories, Albuquerque, NM and Livermore, CA (1997).
7. R. Schulz, J. Huot, G. Liang, S. Boily, G. Lalande, M.C. Denis and J.P. Dodelet, *Mater. Sci. Eng. A* **A276** (1999) 240.
8. M-S. Wu, Y-H Hung, Y-Y. Wang and C-C. Wan, *J. Electrochem. Soc.* **147** (2000) 930.
9. T. Sakai, I. Uehara, and H. Ishikawa, *J. Alloys Compd.* **293–295** (1999) 762.
10. J.J. Reilly, G.D. Adzic, J.R. Johnson, T. Vogt, S. Mukerjee and J. McBreen, *J. Alloys Compd.* **293–295** (1999) 569.
11. P.L. Cabot, E. Guezala, J.C. Calpe, M.T. Garcia and J. Casado, *J. Electrochem. Soc.* **147** (2000) 43.
12. P.L. Cabot, M. Centelles, L. Segarra and J. Casado, *J. Electrochem. Soc.* **144** (1997) 3749.
13. P.L. Cabot, M. Centelles, L. Segarra and J. Casado, *J. Electrochem. Soc.* **145** (1998) 1502.
14. R.C. Hughes, W.K. Schubert and R.G. Buss, *J. Electrochem. Soc.* **142** (1995) 249.
15. Boonsong Sutapun, Massood Tabib-Azar and A. Kazemi, *Sens. Actuators B, chem.* **60** (1999) 27.
16. Chinhua Wang, A. Mandelis and J.A. Garcia, *Sens. Actuators B, Chem.* **60** (1999) 228.
17. A. Sieverts and H. Hagen, *Z. Phys. Chemie A* **174** (1935) 247.
18. A. Sieverts and W. Danz, *Z. Phys. Chemie B* **38** (1937) 61.
19. J.P. Hoare, S. Schuldiner, *J. Phys. Chem.* **61** (1957) 339.
20. T.B. Flanagan and F.A Lewis, *Z. Physik. Chem. Neue Folge* **27** (1961) 104.
21. J.C. Barton and F.A. Lewis, *Trans. Faraday Soc.* **58** (1962) 103.
22. J.C. Barton, A.S. Green and F.A. Lewis, *Trans. Faraday Soc.* **62** (1966) 960.
23. A.W. Carson, F.A. Lewis and W.H. Schurter, *Trans. Faraday Soc.* **63** (1967) 1447.
24. B. Baranowski and R. Wisniewski, *Phys. Stat. Sol.* **35** (1969) 593.

25. R.J. Smith and D.A. Otterson, *J. Phys. Chem. Solids* **31** (1970) 187.
26. F.A. Lewis, K. Kandasamy, R-A. McNichol and X.Q. Tong, *Int. J. Hydrogen Energy* **20** (1995) 369.
27. K. Yamakawa, *J. Phys., Condens. Matter* **11** (1999) 8681.
28. E.S. Kooij, A.T.M. van Gogh and R. Griessen, *J. Electrochem. Soc.* **146** (1999) 2990.
29. S.Y. Qian, B.E. Conway and G. Jerkiewicz, *Int. J. Hydrogen Energy* **25** (2000) 539.
30. D.J.G. Ives and J.G. Janz, 'Reference Electrodes' (Academic Press, New York, 1961, p. 111–116.
31. D.J.G. Ives and J.G. Janz, *op. cit.* [30], pp. 270–321.
32. W.W. Harvey, *J. Electrochem. Soc.* **109** (1962) 638.
33. R.I. Tucceri and D. Posadas, *J. Electrochem. Soc.* **128** (1981) 1478.
34. G. Busca, Thesis, University of Milan Italy (1996).
35. Kirk-Othmer, 'Encyclopedia of Chemical Technology', Vol. 10 (J. Wiley & Son, New York, 1966, 2nd edn), p. 682.
36. H.C. Jamieson and F.D. Manchester, *J. Phys. F, Met. Phys.* **2** (1972) 323.
37. B. Stritzker and W. Buckel, *Z. Physik.* **257** (1972) 1.
38. E. Wicke, H. Brodowsky, with cooperation by H. Züchner, *in* G. Alefeld and J. Volkl (Eds), 'Topics in Applied Physics', Vol. 28 (Springer-Verlag, Berlin, 1978), p. 73.
39. N. Ibl, *in* E. Yeager, J.O'M. Bockris, B.E. Conway and S. Sarangapani (Eds), 'Comprehensive Treatise of Electrochemistry' Vol. 6 (Plenum Press, New York, 1983), pp. 238–315.
40. N. Ibl, *op. cit.* [39], p. 243.